Heterogeneous Formation of Particulate Nitrate under Ammonium-rich Regime during the High $PM_{2.5}$ Events in Nanjing, China

Yu-Chi Lin[1,2,3], Yan-Lin Zhang[1,2,3*], Mei-Yi Fan[1,2,3], Mengying Bao[1,2,3]

[1.] Yale-NUIST Center on Atmospheric Environment, International Joint Laboratory on Climate and Environment Change, Nanjing University of Information Science and Technology, Nanjing, 210044, China.

[2.] Key Laboratory Meteorological Disaster; Ministry of Education & Collaborative Innovation Center on Forecast and Evaluation of Meteorological Disaster, Nanjing University of Information Science and Technology, Nanjing, 210044, China.

[3]. Jiangsu Provincial Key Laboratory of Agricultural Meteorology, College of Applied Meteorology, Nanjing University of Information Science & Technology, Nanjing 210044, China.

Corresponded to Yan-Lin Zhang (dryanlinzhang@outlook.com; zhangyanlin@nuist.edu.cn)

ABSTRACT

Particulate nitrate (NO_3^-) not only influences regional climates but also contributes to the acidification of terrestrial and aquatic ecosystems. In 2016 and 2017, four intensive online measurements of water-soluble ions in $PM_{2.5}$ were conducted in Nanjing City to investigate the potential formation mechanisms of particulate nitrate. During the sampling periods, NO_3^- was the most predominant species, accounting for 35 % of the total water-soluble inorganic ions, followed by SO_4^{2-} (33 %) and NH_4^+ (24 %). Significant enhancements of nitrate aerosols in terms of both absolute concentrations and relative abundances suggested that NO_3^- was a major contributing

species to high-$PM_{2.5}$ events (hourly $PM_{2.5}$ $\geqq$ 150 μg m^{-3}). High NO_3^- concentrations mainly occurred under NH_4^+-rich conditions, implying that the formation of nitrate aerosols in Nanjing involved NH_3. During the high-$PM_{2.5}$ events, the nitrogen conversion ratios (Fn) were positively correlated with the aerosol liquid water content (ALWC, $R > 0.72$, $p < 0.05$). Meanwhile, increasing NO_3^- concentrations regularly coincided with increasing ALWC and decreasing Ox (Ox = O_3 +NO_2). These results suggested that the heterogeneous reaction was probably a major mechanism of nitrate formation during the high-$PM_{2.5}$ events. Moreover, the average production rate of NO_3^- by heterogeneous processes was estimated to be 12.6 % h^{-1} (4.1 μg m^{-3} h^{-1}), which was much higher than that (2.5 % h^{-1}, 0.8 μg m^{-3} h^{-1}) of gas-phase reactions. This can also explain the abrupt increase of nitrate concentrations during the high $PM_{2.5}$ events. Utilization of ISORROPIA II model, we found that nitrate aerosol formation in Nanjing during the high-$PM_{2.5}$ events was HNO_3-limited. This indicated that the control of NOx emissions will be able to efficiently reduce airborne nitrate concentrations and improve the air quality in this industrial city.
Keywords: Nitrate aerosols, nitrogen conversion ratios, NH_4^+-rich regime, Hydrolysis of N_2O_5, Nitrate production rate

1. Introduction

Due to the rapid growth of industrialization and urbanization, particulate matter (PM) pollution has become a severe problem in China in recent years (Chan and Yao, 2008; Zhang and Cao, 2015). Fine mode particles ($PM_{2.5}$, with aerodynamic diameters less than 2.5 μm) exhibit smaller sizes and contain many toxins emitted from anthropogenic emissions (Huang et al., 2018). $PM_{2.5}$ easily penetrates the upper respiratory tract and is deposited into the human body, causing serious threats to human health. Numerous previous studies have proven that people exposed to high

52 $PM_{2.5}$ concentrations show increased risks of respiratory illness, cardiovascular
53 diseases and asthma (Brauer et al., 2002; Defino et al., 2005), resulting in an increase
54 of mortality (Nel, 2005).

55 Secondary inorganic aerosols (SIA), including sulfate (SO_4^{2-}), nitrate (NO_3^-) and
56 ammonium (NH_4^+), are major constituents of $PM_{2.5}$, accounting for 25 - 60 % of the
57 $PM_{2.5}$ mass in urban cities of China (Huang et al.,2014a; Wang et al., 2018; Yang et
58 al., 2005; Ye et al., 2017; Zhao et al., 2013; Zhou et al., 2018). Among these species,
59 SO_4^{2-} and NO_3^- are acidic ions which tend to be neutralized by NH_4^+. Previously,
60 many studies suggested that SO_4^{2-} dominated SIA in urban cities of China (Kong et
61 al., 2014; Tao et al., 2016; Yang et al., 2005; Yao et al., 2002; Zhao et al., 2013). In
62 recent years, the Chinese government reduced its anthropogenic emissions by 62 %
63 and 17 % for SO_2 and NOx, respectively (Zheng et al., 2018). This revealed that the
64 reduction efficiency of SO_2 emissions were much higher than those of NOx.
65 Consequently, nitrate has become the dominant species of SIA, especially during PM
66 haze events (Wang et al., 2018; Wen et al., 2015; Zou et al., 2018).

67 In the atmosphere, ammonium nitrate (NH_4NO_3) is a major form of nitrate
68 aerosols in fine mode particles. NH_4NO_3 is a semi-volatile species which partitions
69 from the particle phase into the gas phase under high-temperature (T) conditions. It
70 deliquesces when the ambient relative humidity (RH) is higher than its deliquescence
71 relative humidity (DRH, nearly 62 % RH at atmospheric standard condition). To
72 produce NH_4NO_3, nitrogen oxides (NO_x) and ammonia (NH_3) undergo a series of
73 chemical reactions. NO_x mostly emits as fresh NO, which is subsequently oxidized to
74 NO_2 and reacts with hydroxyl (OH) radicals to generate nitric acid (HNO_3), and then
75 HNO_3 reacts with NH_3 to yield NH_4NO_3 particles as listed in R1 and R2 (Calvert and
76 Stockwell, 1983). Particulate NH_4NO_3 formation rate is profoundly dependent on the
77 ambient T and RH since both parameters influence the equilibrium constant of NO_3^-

and NH_4^+ between the particle and gas phases, as listed in R2 (Lin and Cheng, 2007).

$$NO_{2(g)} + OH_{(g)} \rightarrow HNO_{3(g)} \qquad k_1 \qquad (R1)$$

$$HNO_{3(g)} + NH_{3(g)} \rightarrow NH_4NO_{3(s,\,aq)} \qquad k_2 \qquad (R2)$$

Here, k_1 and k_2 are the reaction rate and equilibrium constant of R1 and R2, respectively. The equilibrium constant k_2 can be expressed as the product of HNO_3 and NH_3.

Heterogeneous reactions have been considered an important mechanism of nitrate formation during the nighttime. As listed in R3, liquid HNO_3 is produced by the hydrolysis of dinitrogen pentoxide (N_2O_5) on aerosol surfaces (Brown & Stutz, 2012; Chang et al., 2011; Mental et al., 1999; Wahner et al., 1998). Liquid HNO_3 can be neutralized by NH_4^+, which is produced from the conversion of gaseous NH_3. Nitrate aerosols yielded from both R2 and R3 require NH_3, and we can therefore consider these processes of NO_3^- formation to occur under NH_4 -rich conditions. Sometimes, there is not enough NH_3 (NH_4^+) to react (to be neutralized) with HNO_3 (NO_3^-) after complete neutralization by H_2SO_4. Under this condition, HNO_3 tends to react (or to be neutralized) with other alkaline species such as Ca-rich dust ($CaCO_3$), and subsequently, nitrate aerosol is produced under a NH_4^+-poor regime (Goodman et al., 2000).

$$N_2O_{5(g)} + H_2O_{(l)} \rightarrow 2HNO_{3(aq)} \qquad (R3)$$

The Yangtze River Delta (YRD) region is one of the well-known polluted areas in China (Zhang and Cao, 2015). Different from the case of dramatic elevated sulfate aerosol levels in Beijing (Wang et al., 2016), nitrate aerosols seemed to be a major contributing species during haze days in the YRD region (Wang et al., 2015; Wang et al., 2018). The formation mechanisms of nitrate in Nanjing have not yet been well understood, especially during high PM events. In this study, four intensive online

104 measurements of water-soluble ions in $PM_{2.5}$ were conducted in Nanjing City in 2016
105 and 2017. The data provided information on the hourly evolution of water-soluble
106 inorganic ions (WSIIs) in the industrial city. The NO_3^- distributions under different
107 NH_4^+ regimes (NH_4^+-poor and NH_4^+-rich conditions) were also discussed. Finally, we
108 investigated the potential formation mechanisms of nitrate aerosols and their
109 production rates during high-$PM_{2.5}$ events based on the online measurements.
110
111 **2. Methodology**
112 **2.1 Sampling site**
113 Particulate WSIIs and inorganic gases were continuously monitored at Nanjing
114 University of Information Science and Technology (NUIST) located in the northern
115 part of Nanjing City (see Figure S1). In addition to the contributions from vehicle
116 emissions, petroleum chemical refineries and steel manufacturing plants are situated
117 in the northeast and east direction at a distance of approximately 5 km. Four intensive
118 campaigns were conducted from March 2016 to August 2017. During each
119 experiment, the hourly concentrations of WSIIs in $PM_{2.5}$ and inorganic gases were
120 continuously observed. Meanwhile, the hourly $PM_{2.5}$, NO_2 and O_3 concentrations
121 along with the ambient T and RH were acquired from the Pukou air quality
122 monitoring station which is located to the southwest of the receptor site.
123
124 **2.2 Instruments**
125 To monitor the hourly concentrations of WSIIs (Cl^-, NO_3^-, SO_4^{2-}, Na^+, NH_4^+, K^+,
126 Mg^{2+} and Ca^{2+}), an online Monitor for Aerosols and Gases (MAGAR, Applikon-ENC,
127 The Netherlands) instrument with a $PM_{2.5}$ inlet was employed. Using this instrument,
128 the WSIIs in $PM_{2.5}$ were collected by a stream jet aerosol collector, while acidic (HCl,
129 HONO, HNO_3 and SO_2) and basic gases (NH_3) were dissolved in a hydrogen peroxide

solution on a wet rotation denuder (ten Brink et al., 2007; Griffith, et al., 2015). The liquid samples were then collected with syringe pumps and analyzed by ion chromatography (IC). Before each campaign, a seven-point calibration curve of each species was made, and an internal standard solution (LiBr) was used to check instrumental drifts. The method detection limits (MDLs) of Cl^-, NO_3^-, SO_4^{2-}, Na^+, NH_4^+, K^+, Mg^{2+} and Ca^{2+} were, 0.01, 0.04, 0.06, 0.05, 0.05, 0.07, 0.05 and 0.11 μg m^{-3}, respectively. For gases, the MDLs were 0.07, 0.09, 0.06, 0.02 and 0.08 μg m^{-3} for HCl, HONO, HNO_3, SO_2 and NH_3, respectively.

2.3 ISORROPIA-II model

In this work**,** we used the ISORROPIA-II model to calculate the aerosol liquid water content (ALWC). ISORROPIA II is a thermodynamic equilibrium model which is built based on the Na^+ - Cl^- - Ca^{2+} - K^+ - Mg^{2+} - SO_4^{2-} - NH_4^+ - NO_3^- - H_2O aerosol system (Fountoukis & Nenes, 2007). This model has been successfully used to estimate the liquid water content in aerosols with uncertainty of ~ 20 % compared to the observed ALWC (Bian et al., 2014; Guo et al., 2015; Liu et al., 2017). This underestimation might be due to the missed species in ISORROPIA II, organic aerosols, , which contributed approximately 27 % of the total ALWC (Bougiatioti et al., 2007). Here, the model was computed as a "forward problem", in which the quantities of aerosol- and gas-phase compositions along with the T and RH were well known. Additionally, the modeled values were determined using the "metastable" mode, which indicated that the aerosol compositions were assumed to be composed of an aqueous solution (Liu et al., 2017). The details of this model can be found elsewhere (Fountoukis and Nenes, 2007). In this work, the observed concentrations of total nitrate (HNO_3+NO_3^-), total ammonium (NH_3 + NH_4^+), total chloride (HCl + Cl-), SO_4^{2-}, Na^+, K^+, Mg^{2+} and Ca^{2+} along with measured ambient T and RH served as

input of ISORROPIA II model.

2.4 Potential source contribution function

Potential source contribution function (PSCF) is a method to identify the potential source regions of air pollutants. It has also been widely used to differentiate local emission from long-range transported pollution (Zhang et al., 2013; Hui et al., 2018) based on the trajectory analysis calculated from GDAS (Global Data Assimilation System), which processed by the National Centers for Environmental Prediction (NCEP). The zone of concern is divided into $i \times j$ small equal grid cells and then PSCF in the *i-jth* cell ($PSCF_{ij}$) can be defined as (Polissar et al., 1999):

$$PSCF_{ij} = \frac{m_{ij}}{n_{ij}} \quad (1)$$

where m_{ij} is the number of "high nitrate pollution" trajectory endpoints in the *i-jth* cell and n_{ij} is the total number of trajectory endpoints fallen into the *i-jth* cell. In this study, the 80th percentile value of nitrate concentration was treated as "high nitrate pollution" threshold. To reduce the uncertainty caused by the small values of n_{ij}, the weighting function of W_{ij} has to be considered (Polissar et al., 1999):

$$W_{ij} = \begin{cases} 1.00; & 80 < n_{ij} \\ 0.70; & 20 < n_{ij} \leqq 80 \\ 0.42; & 10 < n_{ij} \leqq 20 \\ 0.05; & n_{ij} \leqq 10 \end{cases}$$

In this study, the domain of the study area was in a range of 20-55 °N and 105-135 °E; the resolution of grid cell was 0.5°×0.5°.

3. Results and discussion

3.1 Overview of water-soluble inorganic ions

Four intensive online measurements of WSIIs in $PM_{2.5}$ were carried out in Nanjing City from March 2016 to August 2017. Figure 1a plots the time series of the hourly $PM_{2.5}$ mass concentrations during the sampling periods. As seen, the hourly $PM_{2.5}$ mass concentrations varied from 5 to 252 μg m^{-3} with a mean value of 58 ± 35 μg m^{-3}. Compared with the 24-hour guideline (25 μg m^{-3}) suggested by the World Health Organization (WHO), our average $PM_{2.5}$ concentration (58 μg m^{-3}) was 2.3 times higher. This indicated that PM pollution in Nanjing City was a serious problem. During the campaigns, several high-$PM_{2.5}$ events with hourly $PM_{2.5}$ concentrations of higher than 150 μg m^{-3} were observed in the springtime and wintertime. These high $PM_{2.5}$ levels lasted for more than 3 hours, with obviously elevated NO_3^-. The details of nitrate formation during the high-$PM_{2.5}$ hours will be discussed in the following sections.

Figure 1b shows the time series of the hourly concentrations of SIA species, including SO_4^{2-}, NO_3^- and NH_4^+. The lack of data from March 7 to 14, 2016 was due to a malfunction of the MARGA instrument. During the sampling periods, the NO_3^- concentrations varied from 0.1 to 85.1 μg m^{-3} with a mean value of 16.7 ± 12.8 μg m^{-3}. The SO_4^{2-} concentrations ranged from 1.7 to 96.2 μg m^{-3} and averaged 14.9 ± 9.1 μg m^{-3}. The NH_4^+ concentrations fluctuated between 0.8 and 44.9 μg m^{-3} with a mean value of 10.7 ± 6.7 μg m^{-3}. On average, SIA accounted for 91 % of the total water-soluble inorganic ions (TWSIIs) during the entirety of the sampling periods (see Figure 2a). Among these species, NO_3^- accounted for 35 % of the TWSIIs, followed by SO_4^{2-} (33 %) and NH_4^+ (24 %). The abundances of other ions, including Cl^-, K^+, Ca^{2+}, Na^+ and Mg^{2+}, were 5, 2, 1, 0.7 and 0.3 %, respectively. Figure S2 shows the scatter plot of the equivalent concentrations of the cations (Na^+, NH_4^+, K^+, Mg^{2+} and

207 Ca^{2+}) and anions (Cl^-, SO_4^{2-} and NH_4^+). As seen, good correlations (R = 0.98 -0.99,
208 with a significance level $p<0.05$) between cations and anions were found during the
209 various sampling periods. The ratio of cation-to-anion was very close to 1.0 during
210 each season, reflecting an ionic balance. This also indicated that our data exhibited
211 good quality and was able to be used for the further analysis of scientific issues.
212 All SIA species exhibited similar seasonal patterns, with lower concentrations in
213 the summer, especially for NO_3^-. The average concentrations of nitrate were 6.7 and
214 5.7 μg m^{-3} in the summertime of 2016 and 2017, respectively (see Figure S3). These
215 values were much lower than those observed during other seasons. The local
216 meteorological conditions, which were favorable for the dilution of air pollution, were
217 one of the reasons for the declined NO_3^- concentrations during the hot seasons (Zhang
218 and Cao, 2015). Another important reason for this effect was attributed to the
219 formation process of $PM_{2.5}$ nitrate, which is very sensitive to the ambient T and RH
220 (Lin and Cheng, 2007). Figure S4a depicts the theoretical equilibrium constants of
221 partitioned NO_3^- and NH_4^+ between the particle and gas phase ($HNO_{3(g)} + NH_{3(g)} \rightarrow$
222 $NH_4NO_{3(s, aq)}$ as seen in R2) under different T and RH conditions. The details of
223 calculation approach of the theoretical equilibrium constants are described in
224 *Supplementary S1*. Note that the *Y-axis* is presented on a log scale. The theoretical
225 equilibrium constants increased exponentially with increasing ambient temperature
226 but decreased with increasing RH. This indicated that NH_4NO_3 would be partitioned
227 into the gas phase due to high equilibrium constants under high-temperature and low-
228 RH conditions. Figure S4b illustrates the time series of the theoretical and observed
229 equilibrium constants during the sampling periods. As can be seen, most of the
230 observed equilibrium constants were higher than the theoretical ones, suggesting that
231 NH_4NO_3 aerosols were produced in Nanjing during the sampling periods. Obviously,
232 higher theoretical and lower observed equilibrium constants were found during the

summer. This suggested that more NO_3^- and NH_4^+ would tend to be partitioned into the gas phase, resulting in lower particulate nitrate concentrations during hot seasons (Lin and Cheng, 2007).

Apart from seasonal variations, pronounced diurnal patterns were also found for SIA species (see Figure 3). NO_3^- exhibited similar diel cycles during different seasons, with higher concentrations in the early morning (3 a.m. - 7 a.m.) and lower levels between 2 p.m. and 5 p.m. The high nitrate concentrations in the early morning might be caused by the nitrate formation via heterogeneous reaction in the dark, and gas-phase oxidation after sunrise and the subsequent condensation on pre-existing particles before the temperature increased and RH decreased afterwards. Moreover, the lower planet boundary layer (PBL) might be another reason for enhanced nitrate in the early morning. However, the lower concentrations of nitrate during the daytime might be attributed to the higher PBL, and high temperatures, which inhibited the build-up of nitrate, especially during the summertime. In terms of sulfate, higher concentrations were observed between 6 am. and 1 p.m., indicating that the formation rate of sulfate was higher than the removal/dilution rate, leading to an increase of the sulfate concentration during the daytime. The diurnal patterns of NH_4^+ mimicked those of NO_3^-, showing lower concentrations during the daytime. This was explained by the drastic decrease of particulate NH_4NO_3 concentrations under high temperatures and low relative humidity, resulting in lower NH_4^+ levels during the daytime.

3.2 Enhancements of nitrate at high $PM_{2.5}$ levels

Figure S5 shows the scatter plots of NO_3^-, SO_4^{2-} and NH_4^+ against $PM_{2.5}$. As seen, the slopes of NO_3^- (NO_3^- vs. $PM_{2.5}$ mass), SO_4^{2-} and NH_4^+ were 0.30, 0.24 and 0.19, respectively. This suggested that the increasing rate of NO_3^- during the high-$PM_{2.5}$ events was higher than those of other SIA species. At high $PM_{2.5}$ levels ($PM_{2.5} \geq$

150 μg/m^3), NO_3^-, SO_4^{2-} and NH_4^+ contributed 39, 28 and 24 % of the TWSIIs, respectively (Figure 2b). However, the relative abundances of NO_3^-, SO_4^{2-} and NH_4^+ during low $PM_{2.5}$ concentrations (hourly $PM_{2.5}$ < 35 μg/m^3, see Figure 2c) were 29, 37 and 23 %, respectively. In recent years, dramatically enhanced amounts of nitrate aerosols during high-PM events have been observed at many urban sites in China (Wen et al., 2015; Wang et al., 2017; 2018; Zou et al., 2018). For instance, Zou et al. (2018) found that the nitrate concentrations during the occurrence of polluted air in Beijing and Tianjin were almost 14 times higher than those on relatively clean days ($PM_{2.5}$ < 75 μg/m^3), and the enhancement ratio of nitrate was much higher than that (5.3) of sulfate. Wang et al. (2018) noted that the enhancement ratio of NO_3^- (~6) between haze and clear days in Ningbo of the YRD region was much higher than that of SO_4^{2-} (~3). These findings suggested that NO_3^- was a major contributing species to fine particles during haze days since its increasing ratio between haze and non-haze days was much higher than those of other SIA species, such as sulfate and ammonium.

3.3 PSCF result of high nitrate pollution

During the high $PM_{2.5}$ pollution, significant enhanced nitrate aerosols in terms of both absolute concentration and relative abundance to TWSIIs were found. Next, we tried to use PSCF analysis to identify whether local emission or long-range transported pollution was the major source of high nitrate concentrations at the receptor site. In this work, the 80th percentile values of nitrate concentration was selected as “high nitrate pollution” threshold for PSCF analysis. Figure 4 plots the PSCF result of high nitrate pollution in Nanjing during the sampling periods. The region corresponding to high PSCF value grid is a potential source region of nitrate aerosols. As can be seen, the areas with high PSCF value (>0.8) were regularly local

areas surrounding by Nanjing while PSCF values from other long-distance areas were lower than 0.2. This suggested that NO_3^- aerosols in Nanjing during the high nitrate pollution were likely from local emissions rather than long-range transported sources.

3.4 Nitrate formation under different ammonium regimes

Ammonium is a major species that neutralizes particulate SO_4^{2-} and NO_3^-. In the atmosphere, SO_4^{2-} competes with NO_3^- for NH_4^+ during their formation processes, and therefore, the relationship between the molar ratios of NO_3^-/SO_4^{2-} and NH_4^+/SO_4^{2-} can give us a hint for understanding the formation of NO_3^- under different ammonium regimes (Pathak et al., 2009; He et al., 2012; Tao et al., 2016). In an ammonium-rich regime, the HNO_3 produced by both gas oxidation and heterogeneous process reacts (or neutralizes) with "excess-ammonium" (excess-NH_4^+) at a NH_4^+/SO_4^{2-} molar ratio > 2 (theoretical value in an NH_4^+-rich regime) when sulfate is completely neutralized by NH_4^+ to form $(NH_4)_2SO_4$ (Squizzato et al., 2013; Ye et al., 2011). In contrast, nitrate can be found under ammonium-poor conditions with a theoretical NH_4^+/SO_4^{2-} value that should be less than 2 (Pathak et al., 2009). Under NH_4^+-poor conditions, HNO_3 reacts with other cations, such as the calcium carbonate frequently found in natural dust.

Figure 5 shows the scatter plot of the molar ratios of NO_3^-/SO_4^{2-} against NH_4^+/SO_4^{2-}. It is found that good correlations exist between NO_3^-/SO_4^{2-} and NH_4^+/SO_4^{2-} under NH_4^+-rich regimes, with a coefficient of determination (R^2) of 0.84 - 0.94 in the different seasons (see in Table 1). Utilizing the linear regression model, we suggested that nitrate aerosols (in NH_4^+-rich regimes) began to form when the NH_4^+/SO_4^{2-} molar ratios exceeded the criterion values of 1.7-2.0 during the different seasons (Table 1). The criterion value can be calculated as absolute value of "intercept" dividing by slope in each linear regression model (He et al., 2012). The

criterion values below 2 suggested that part of the sulfate might have existed in other forms, such as ammonium bisulfate. On the other hand, under ammonium-rich conditions, nitrate concentrations should be positively proportional to "excess-NH_4^+" concentrations, a relationship which was defined as [excess-NH_4^+] = (NH_4^+/SO_4^{2-} - criterion value) × [SO_4^{2-}] (Pathak et al., 2009) (sulfate is in the units of nmol m^{-3} here). The criterion values were acquired from the regression models, as listed in Table 1. The results revealed that the excess-NH_4^+ concentrations varied from -283 to 1422 nmol m^{-3} (see Figure 6), and only 1 % of data showed deficit-NH_4^+ conditions, reflecting that NO_3^- formation in Nanjing occurred primarily under the NH_4^+-rich conditions. Moreover, the excess-NH_4^+ had apparent diurnal cycles, with higher concentrations in the early morning and lower concentrations at midday and in the early afternoon (see Figure 3, where we converted the units from nmol m^{-3} to μg m^{-3}). The diurnal patterns of NO_3^- mimicked those of the excess-NH_4^+. This also suggested that particulate NO_3^- formation occurred mainly under NH_4^+-rich conditions. Figure 6 illustrates the relationship between the nitrate and excess-NH_4^+ molar concentrations during the sampling periods. The nitrate molar concentrations correlated linearly with the excess-NH_4^+ molar concentrations with a slope of approximately 1.0, which was consistent with the molar ratio of reaction between HNO_3 and NH_3. Interestingly, some scattered points were found in high ammonium concentrations (excess-NH_4^+ $\geqq$ 900 nmol m^{-3} ~ 16.2 μg m^{-3}), implying that residual NH_4^+ might be presented in another form such as NH_4Cl under high-NH_4^+ conditions. On the contrary, NO_3^- aerosols can be produced without involving NH_3; therefore, NO_3^- did not correlate well with the excess NH_4^+ under a NH_4^+-poor regime.

In this study, high nitrate concentrations were always found under NH_4^+-rich regimes, elucidating that nitrate production during high PM levels in Nanjing had to be involved with NH_3 or NH_4^+. Figure 6 also shows the nitrate concentrations against

337 the excess-NH_4^+ observed in various cities of China during the summertime (Pathak et
338 al., 2009; Griffith et al., 2015). In Beijing and Shanghai, high nitrate concentrations
339 during the summertime were found under NH_4^+-deficient conditions, which was very
340 different from the findings of this work. In these studies (Pathak et al., 2009; Griffith
341 et al., 2015), the high nitrate concentrations associated with NH_4^+-poor conditions
342 might be due to the lower excess-NH_4^+ concentrations under high-SO_4^{2-} conditions at
343 that time since the strict control of SO_2 emissions by the Chinese government started
344 in 2010 (Zheng et al., 2018). In recent years, the reduction of anthropogenic SO_2
345 emissions decreased the airborne SO_4^{2-} concentrations, resulting in more excess-NH_4^+
346 and leading to nitrate aerosol formation under NH_4^+-rich regimes. This argument can
347 be supported by the recent results shown in Figure S6, in which high nitrate
348 concentrations in Beijing were always found under NH_4^+-rich regimes.
349
350 **3.5 Nitrate formation mechanism during high-$PM_{2.5}$ episodes**
351 In this section, we attempted to explore the formation mechanisms of nitrate
352 aerosols during high $PM_{2.5}$ levels. Here, nitrogen conversion ratio (Fn) was used to
353 evaluate the conversion capability of NO_2 to total nitrate (TN, TN=HNO_3 + NO_3^-),
354 and it can be defined as (Khoder, 2002; Lin et al., 2006):
355
356 $$F_n = \frac{GNO_3^- + PNO_3^-}{GNO_3^- + PNO_3 + NO_2} \quad (1)$$
357 where GNO_3^- and PNO_3^- represent the NO_2 concentrations in nitric acid and
358 particulate nitrate, respectively, with the units of μg m^{-3}. The results showed that the
359 Fn values during the sampling periods varied from 0.01 to 0.57 with a mean value of
360 0.14 ± 0.09 (see Figure 1e). This value was comparable to that (0.17) in Taichung,
361 Taiwan, where both gas-oxidation and heterogeneous reaction were the dominant
362 formation mechanisms of atmospheric HNO_3 (or NO_3^-) (Lin et al., 2006). However,

363 our Fn value was 2.3 time higher than that (0.06) in Dokki, Egypt (Khoder, 2002).
364 The reason of significant discrepancy of Fn between this work and that in Dokki was
365 not clearly understood, but it might be attributed to different formation processes of
366 HNO_3. In Dokki, gas-phase oxidation was the dominant pathway of HNO_3 production
367 while heterogeneous process (R3) played an important role in HNO_3 formation in
368 addition to gas-phase oxidation in Nanjing, especially during the high-$PM_{2.5}$ events
369 (discussed later). The reaction rate of HNO_3 by heterogeneous process was much
370 higher than that by gas-phase oxidation (Calvert and Stockwell, 1983) and therefore,
371 the Fn value was much higher in this study. On the other hand, Fn displayed
372 significant diurnal cycles, with the highest value in the early morning (see in Figure
373 3). This elevated Fn coincided with increasing ALWC, suggesting heterogeneous
374 reaction since ALWC is one of the key parameters which favors the transformation of
375 N_2O_5 to liquid HNO_3 in this process (also indicated that nitrate formation was
376 associated with heterogeneous process). On the contrary, a second peak of Fn was
377 found in the early afternoon when Ox ($Ox = NO_2 + O_3$, an index of the oxidation
378 capacity) concentrations increased, but ALWC decreased. This suggested that the
379 HNO_3 formation might be mainly associated with the gas-phase reaction of NO_2 +
380 OH during the daytime; also reflected that nitrate formation was via gas-phase
381 oxidation.
382 Assuming that long-range transported nitrate can be neglected in this study (in
383 section 3.3), we attempted to analyze the correlations of Fn vs. OH and Fn vs. ALWC
384 to investigate whether gas-phase oxidation or heterogeneous reactions might be the
385 dominant mechanism of nitrate production. In this work, the OH radical
386 concentrations were not measured; hence, we used O_X as a proxy of OH. The ALWC
387 was acquired by computing the ISOPROPIA II model as described in section 2.3.
388 Figure 7 illustrates the scatter plots of Fn against Ox and ALWC in both daytime and

nighttime aerosol samples during the high-$PM_{2.5}$ events. Fn correlated well with the ALWC, with a correlation coefficient (R) of 0.72 and 0.76 ($p < 0.05$) at daytime and nighttime samples, respectively. However, a poor correlation was found between Fn and Ox (R was 0.17 and 0.52 for the daytime and nighttime samples, $p>0.05$). This implied that nitrate formation during the high-$PM_{2.5}$ events in Nanjing was likely attributed to heterogeneous reactions. This result was consistent with recent conclusions reached by oxygen isotope techniques, in which the hydrolysis of N_2O_5 in preexisting aerosols was found to be a major mechanism of NO_3^- formation (Chang et al., 2018).

3.6 Case study and production rate of NO_3^- during $PM_{2.5}$ episodes

Figure 8 shows several high-$PM_{2.5}$ events observed from March 3 to 6 in 2016. In case I, the high $PM_{2.5}$ concentrations started at 6 p.m. on March 3 and ended at 3 a.m. on March 4. During this event, the SO_4^{2-} and NH_4^+ concentrations remained at almost constant levels, but the NO_3^- concentrations revealed a slight enhancement. In the early morning of March 4, the NO_3^- concentrations increased from 39.4 to 47.8 μg m^{-3} within 4 hours, resulting in a nitrate production rate of 2.3 μg m^{-3} h^{-1} (~5.5 % h^{-1}, the calculation of NO_3^- production rate can be seen in the *Supplementary S2*). In case II, high $PM_{2.5}$ concentrations were observed from 8. a.m. to 2. p.m. on March 4. The NO_3^- concentrations were much higher than those of SO_4^{2-}, indicating nitrate-dominated aerosols. In this case, the NO_3^- concentrations increased from 38.1 to 51.2 μg m^{-3} within 6 hours, suggesting that the increasing rate of NO_3^- was 1.0 μg m^{-3} h^{-1} (2.4 % h^{-1}). Since the high NO_3^- concentrations occurred under high-Ox and low-ALWC conditions, this suggested that the gas-phase reaction of NO_2 + OH might be the dominant source of NO_3^- production in this event. In case III, a rapid growth of the $PM_{2.5}$ mass was found around midnight, along with a dramatic increase of NO_3^-

concentrations from 11 p.m. on March 4 (31.0 μg m^{-3}) and maximizing at 1 a.m. the next day (64.5 μg m^{-3}). The increasing rate of NO_3^- was estimated to be 11.4 μg m^{-3} h^{-1} (~19.5 % h^{-1}), which was much higher than those in case I and II. The high-nitrate event was found under increasing ALWC and decreasing Ox concentration conditions, suggesting that nitrate production occurred through heterogeneous processes. In case IV, the enhancements of all SIA species coincided with increasing ALWC and declining Ox concentrations. Again, the enhancement of nitrate was likely attributed to heterogeneous reactions rather than to gas-phase processes. In these events, the NO_3^- production rate was estimated to be 5.0 μg m^{-3} h^{-1} (~ 15.4 % h^{-1}).

Through the sampling periods, a total of twelve high $PM_{2.5}$ events were found, and the NO_3^- concentrations increased significantly during all the episodes (see in Table S1). Seven episodes suggested that heterogeneous processes (N_2O_5 + H_2O) might be a major pathway for nitrate formation since elevated NO_3^- levels coincided with increasing AWLC and decreasing Ox (or Ox remaining at a constant level). Among these heterogeneous process events, five cases (Case III, Case IX, Case X, Case XI and Case XII in Table S1) were observed during the nighttime (5 p.m. – 6 a.m. on the next day). This suggested that approximately 70 % heterogeneous reaction of nitrate production was observed in the dark. In these events, the average NO_3^- growth rate was 12.6 ± 7.3 % h^{-1} (4.1 ± 3.6 μg m^{-3} h^{-1}). This value was in agreement with those in the literatures which the production rate of nitrate via heterogeneous reaction were 14.3 % h^{-1} by both field measurements and laboratory works (Calvert and Stockwell, 1983; Pathak et al., 2011). On the contrary, NO_3^- concentrations rose with increasing Ox and decreasing ALWC in two $PM_{2.5}$ episodes, indicating gas-phase processes (NO_2 + OH). As listed in Table S1, these gas-phase reaction cases occurred mainly during the daytime. The average production rate of NO_3^- in the gas-oxidation reaction cases averaged 2.5 ± 0.1 % h^{-1} (0.8 ± 0.3 μg m^{-3} h^{-1}), which was in line with that (2.4

441 % h^{-1}) in the subtropical polluted urban site that nitrate aerosols were mainly from
442 gas-oxidation process (Lin et al., 2007). Moreover, we also found some cases in
443 which the elevated NO_3^- might have been from both gas-phase and heterogeneous
444 reactions, and the corresponding NO_3^- growth rate was approximately 7.5 ± 3.0 % h^{-1}
445 (2.5 ± 0.2 μg m^{-3} h^{-1}). In conclusion, enhancements of NO_3^- in Nanjing usually
446 occurred under increased ALWC and decreased Ox conditions, indicating that
447 heterogeneous reactions provided the dominant pathway of nitrate formation during
448 the $PM_{2.5}$ episodes. Moreover, the average growth rate of NO_3^- (12.6 % h^{-1}) by
449 heterogeneous processes was 5 times higher than that (2.5 % h^{-1}) of gas-phase
450 reactions. This might explain the abrupt increase of nitrate concentrations during the
451 high $PM_{2.5}$ events.
452
453 **3.7 HNO_3/NH_3 limitation of nitrate aerosol formation**
454 In Nanjing, high nitrate concentrations occurred mainly under NH_4^+-rich
455 regimes, indicating the involvement of atmospheric NH_3. This also demonstrated that
456 both HNO_3 and NH_3 were crucial precursors for particulate nitrate formation. In this
457 section, we attempted to discuss whether HNO_3 or NH_3 was the limited factor for
458 nitrate formation in Nanjing during the high-$PM_{2.5}$ events. ISORROIPA II model is
459 capable of predicting concentrations of particulate ions in addition to ALWC under
460 thermodynamic equilibrium between gas- and aerosol-phase of these ions (Tang et al.,
461 2016). In section 3.5, we used this model to estimate ALWC. Indeed, the output data
462 also included concentrations of ionic species. Figure S7 illustrates the scatter plots of
463 modeled results against observations of NO_3^-, SO_4^{2-} and NH_4^+ in Nanjing during the
464 sampling periods. Good correlations were found between modeled results and
465 observations (R^2=0.97-0.99 with all slopes of approximately 1.0), suggesting that
466 ISORROPIA II had a good performance in prediction of SIA species. As a result, we

can use ISORROPIA II model to test sensitivity of HNO_3 and NH_3 to particulate nitrate concentrations (Guo et al., 2018).

Figure 7 shows the contour plot of the simulated nitrate concentrations depending on the various total nitrate (TN) and total ammonium (TA, TA=NH_3 + NH_4^+) levels under thermodynamic equilibrium conditions computed by ISORROPIA II model. The details of considered chemical reactions in ISORROPIA II model can be seen elsewhere (Fountoukis & Nenes, 2007). Here, sulfate concentrations were assumed to be 10 and 60 μg m^{-3} for the tests of different sulfate conditions. The average concentrations of total chloride (HCl + Cl^-, 1.3 μg m^{-3}), Na^+ (0.2 μg m^{-3}), K^+ (0.8 μg m^{-3}), Mg^{2+} (0.1 μg m^{-3}) and Ca^{2+} (0.5 μg m^{-3}) along with ambient T (20 °C) and RH (62 %) at the receptor site during the sampling period served as input data in this model. The results showed that the lower simulated NO_3^- concentrations was found in the higher SO_4^{2-} case. This was attributed to less NH_4NO_3 formation under higher SO_4^{2-} conditions since SO_4^{2-} would compete with NO_3^- for NH_4^+.

According to the simulated results, we can roughly split the plots into two parts: one is HNO_3-limited area (right), and another is NH_3-limited region (left). The observed TN and TA concentrations (pink circles) in Nanjing are also plotted in this figure. Most of the observed data sets were mainly affected by TN under a low-SO_4^{2-} case. Under a high-SO_4^{2-} condition, the observed data fell into TA-limited under a low-TN and -TA regime, but fell into TN-limited in high-TA and-TN regimes. During the sampling period, high nitrate concentrations always accompanied with high TN and TA levels, highlighting that nitrate aerosol production in Nanjing during the high $PM_{2.5}$ levels was mainly control by HNO_3. Therefore, control of NOx emissions, which reduced HNO_3 concentrations, might be an important way to decrease airborne nitrate concentrations and ameliorate the air quality in Nanjing.

4. Conclusion and remarks

Four intensive online measurements of water-soluble ions in $PM_{2.5}$ were carried out in Nanjing City in 2016 and 2017 to realize the evolutions of SIA and the potential formation mechanisms of particulate nitrate. During the sampling periods, the average concentrations of NO_3^-, SO_4^{2-} and NH_4^+ were 16.7, 14.9 and 10.7 μg m^{-3}, respectively. This indicated that NO_3^- dominated the SIA. Significant seasonal variations and diurnal cycles were found for all SIA species. The low NO_3^- concentrations observed during the summer daytime could be attributed to the enhanced theoretical and declined observed equilibrium constants of NO_3^- and NH_4^+ between gas- and particle-phase. Obvious enhancements of NO_3^- were found in terms of both absolute concentrations and relative abundances during the $PM_{2.5}$ episodes, indicating that NO_3^- was a major contributing species to $PM_{2.5}$. Different from the results obtained in Beijing and Shanghai, high nitrate concentrations always occurred under NH_4^+-rich regimes. The nitrogen conversion ratio, Fn, correlated well with the ALWC but not with Ox during high-$PM_{2.5}$ episodes. These findings indicated that NO_3^- aerosols at the receptor site were mainly produced by heterogeneous reactions ($N_2O_5 + H_2O$) with the involvement of NH_3. The average production rate of NO_3^- from heterogeneous reactions was estimated to be 12.6 % h^{-1}, which was 5 time higher than that of gas-phase reactions. According to the observations and ISORROPIA II simulated results, particulate nitrate formation in Nanjing was HNO_3-limited, suggesting that the control of NOx emissions will be able to decrease the nitrate concentration and improve the air quality in this industrial city.

During the last decade, the mass ratios of nitrate-to-sulfate in $PM_{2.5}$ in the YRD region have been found to range from 0.3 to 0.7 (Lai et al., 2007; Wang et al., 2003; 2006; Yang et al., 2005; Yao et al., 2002), reflecting that the SO_4^{2-} concentration was much higher than the NO_3^- concentration. In the current study, the average mass ratio

of nitrate-to-sulfate was 1.1. Indeed, high nitrate-to-sulfate mass ratios of > 1 were also observed in other mega-cities of China recently (Ge et al., 2017; Wei et al., 2018; Ye et al., 2017; Zou et al., 2018). The elevated nitrate-to-sulfate ratio should be due to the dramatic reduction of SO_2 emissions. The enhanced ratio also suggests that we should pay more attention to and develop some strategies for the reduction of NOx emissions, leading to declined nitrate concentrations in the atmosphere and improvement of the air quality in China.

Data availability

All the data used in this paper are available from the corresponding author upon request (dryanlinzhang@outlook.com or zhangyanlin@nuist.edu.cn).

Author contributions

YLZ conceived and designed the study. YCL analyzed the data and wrote the manuscript with YLZ. FM and MB performed aerosol sampling and data analyses with YCL.

Competing interests

The authors declare that they have no conflict of interest.

Acknowledgements

This study was financially supported by the National Key R&D Program of China (Grant No. 2017YFC0212700), the Natural Scientific Foundation of China (Nos. 41761144056, 91644103 and 41977185) and Jiangsu Innovation & Entrepreneurship Team.

References

Baasandorj, M., Hoch, S. W., Bares, R., Lin, J. C., Brown, S. S., Millet, D. B., Martin, R., Kelly, K., Zarzana, K. J., Whiteman, C. D., Bube, W. P., Tonnesen, G., Jaramillo, J. C. and Sohl, J.: Coupling between chemical and meteorological processes under persistent coal-air poor conditions: evolution of wintertime $PM_{2.5}$ events and N_2O_5 observation in Utah's Salt Lake Valley. *Environ. Sci. Technol.*, **51**, 5941-5950, https://doi.org/10.1021/acs.est.6b06603, 2017.

Bian, Y. X., Zhao, C. S., Ma, N., Chen, J., and Xu, W. Y.: A study of aerosol liquid water content based on hygroscopicity measurements at high relative humidity in the Northern China Plain. *Atmos. Chem. Phys.,* **14**, 6417-6426, https://doi.org/10.5194/acp-14-6417-2014, 2014.

Bougiatioti, A., Nikolaou, P., Stavroulas, I., Kouvarakis, G., Weber, A., Nenes, R., Kanakidou, M., and Mihalopoulos, N.: Particle water and pH in the eastern Mediterranean: source variability and implication of nutrient availability. *Atmos. Chem. Phys.,* **16**, 4579-4591, https://doi.org/10.5194/acp-7-4639-2007, 2007.

Brauer, M., Hoek, G., Vliet, V. P., Meliefste, K., Fischer, P. H., Wijga, A., Koopman, L. P., Neijens, H. J., Gerritsen, J., Kerkhof, M., Heinrich, J., Bellander, T., and Brunekreef, B.: Air pollution from traffic and the development of respiratory infections and asthmatic and allergic symptoms in children. *Am. J. Respir. Crit. Care Med.*, **166**, 1092-1098, https://doi.org/10.1146/rccm.200108-007OC, 2002.

Brown, S. S., and Stutz, J.: Nighttime radical observation and chemistry. *Chem. Soc. Rev.*, **41**, 6405-6447, https://doi.org/10.1039/c2cs35181a, 2012.

Calvert, J. G., and Stockwell, W. R.: Acid generation in the troposphere by gas-phase chemistry. *Environ. Sci. Technol.*, **17**, 428-443, https://doi.org/10.1021/es00115a727, 1983.

Chan, C. K., and Yao, X.: Air pollution in mega cities in China. *Atmos. Enviro.,* **42**, 1-

42, https://doi.org/10.1016/j.atmosenv.2007.09.003, 2008.

Chang, W. L., Bhave, P. V., Brown, S. S., Riemer, N., Stutz, J., and Dabdub, D.: Heterogeneous atmospheric chemistry, ambient measurements, and model calculations of N_2O_5: a review. *Aerosol Sc. Technol.*, **45**, 655 - 685, https://doi.org/10.1080/02786826.2010.551672, 2011.

Defino, R. J., Siotuas, C., and Malik, S.: Potential role of ultrafine particles in associations between airborne particle mass and cardiovascular health. *Environ. Health Perspect.*, **113**, 934-938, https://doi.org/10.1289/ehp.7938, 2005.

Fountoukis, C., and Nenes, A.: ISORROPIA II: a computationally efficient thermodynamic equilibrium model for K^+-Ca^{2+}-Mg^{2+}-NH_4^+-Na^+-SO_4^{2-}-NO_3^--Cl^--H_2O. *Atmos. Chem. Phys.*, **7**, 4639-4659, https://doi.org/10.5194/acp-7-4639-2007, 2007.

Ge, X., Li, L., Chen, Y., Chen, H., Wu, D., Wang, J., Xie, X., Ge, S., Ye, Z., Xu, J., and Chen, M.: Aerosol characteristics and sources in Yangzhou, China resolved by offline aerosol mass spectrometry and other techniques. *Environ. Pollut.*, **225**, 74-85, https://doi.org/10.1016/j.encpol.2017.03.044, 2017.

Goodman, A. L., Underwood, G. M., and Grassian, V. H.: A laboratory study of the heterogeneous reaction of nitric acid on calcium carbonate particles. *J. Geophys. Res. Atmos.,* **105**, 29053-29064, https://doi.org/10.1029/2000JD900396, 2000.

Griffith, S. M., Huang, X. H. H., Louie, P. K. K., and Yu, J. Z.: Characterizing the thermodynamic and chemical composition factors controlling $PM_{2.5}$ nitrate: Insights from two years of online measurements in Hong Kong. *Atmos. Environ.*, **122**, 864-875, https://doi.org/10.1016/ j.atmosenv.2015.02.009, 2015.

Guo, H., Xu, L., Bougiatioti, A., Cerully, K. M. , Capps, S. L., Heti Jr., J. R., Carton, A. G., Lee, S.-H., Bergin, M. H., Ng, N. L., Nenes, A., and Weber, R. J.: Fine particle water and pH in the southeastern United States. *Atmos. Chem. Phys.*, **15**,

5221-5228. https://doi.org/10.5194/acp-15-5211-2015, 2015.

Guo, H., Otjes, R., Schlag, P., Kiendler-Schar, A., Nenes, A., and Weber, R. J.: Effectiveness of ammonia reduction of control of fine particulate nitrate. *Atmos. Chem. Phys.*, **18**, 12241-12256. https://doi.org/10.5194/acp-18-12241, 2018, 2018.

He, K., Zhao, Q., Ma, Y., Duan, F., Yang, F., Shi, Z., and Chen, G.: Spatial and seasonal variability of $PM_{2.5}$ acidity at two Chinese megacities: insights into the formation of secondary inorganic aerosols. *Atmos. Chem. Phys.*, **12**, 1377-1395. https://doi.org/10.5194/acp-12-1377-2012, 2012.

Huang, R.-J., Zhang, Y., Bozzetti, C., Ho, K.-F., Cao, J.-J., Han, Y., Daellenbach, R., Slowik, J. G., Platt, S. M., Canonaco, F., Zotter, P., Wolf, R., Pieber, S. M., Bruns, E. A., Crippa, M., Ciarelli, G., Piazzalunga, A., Schwikkowski, M., Abbaszade, G., Schnelle-Kreis, J., Zimmerman, R., An, Z., Szidat, S., Baltensperger, U., Haddad, I. E., and Prévôt, A. H.: High secondary aerosol contribution to particulate pollution during haze events in China. *Nature*, **514**, 218-222, https://doi.org/10.1038/nature13774, 2014a.

Huang, R. J., Chen, R., Jing, M., Yang, L., Li, Y., Chen, Q., Chen, Y., Yan, J., Lin, C., Wu, Y., Zhang, R., Haddad, J. E., Prevot, A. S. H., O'Dowd, C. D., and Cao, J.: Source-specific health risk analysis on particulate trace elements: coal combustion and traffic emission as major contributors in wintertime Beijing. *Environ. Sci. Technol. 52,* 10967-10974, https://doi.org/10.1021/acs.est.8b02091.

Huang, Y., Shen, H., Chen, H., Wang, R., Zhang, Y., Su, S., Chen, Y., Lin, N., Zhong, Q., Wang, X., Liu, J., Li, B., Liu, W., and Tao, S.: Quantification of global primary emissions of $PM_{2.5}$, PM_{10} and TSP from combustion and industrial process sources. *Environ. Sci. Technol.,* **48**, 13834-13843, https://doi.org/10.1021/es503696k, 2014b.

623 Hui, L., Liu, X., Tan, Q., Feng, M., An. J., Qu, Y., Zhang, Y., and Jiang, M.:
624 Characteristics, source apportionment and contribution of VOCs to ozone
625 formation in Wuhan, Central China. *Atmos. Environ.,* **192**, 55-71,
626 https://doi.org/10.1016/j.atmosenv.2018.08.0642, 2018.
627 Khoder, M. I.: Atmospheric conversion of sulfur dioxide to particulate sulfate and
628 nitrogen dioxide to particulate nitrate and gaseous nitric acid in an urban area.
629 *Chemosphere*, **49**, 675-684, https://doi.org/10.1016/S0045-6535(02)00391-0,
630 2002.
631 Kong, L., Yang, Y., Zhang, S., Zhao, X., Du, H., Fu, H., Zhang, S., Cheng, T., Yang,
632 X., Chen, J., Wu, D., Sheng, J., Hong, S., and Jiao, L.: Observation of linear
633 dependence between sulfate and nitrate in atmospheric particles. *J. Geophys. Res.*
634 *Atmos.,* **119**, 341-361, https://doi.org/10.1002/2013JD020222, 2014.
635 Lin, Y.-C., and Cheng, M.-T.: Evaluation of formation rates of NO_2 to gaseous and
636 particulate nitrate in the urban atmosphere. *Atmos. Environ.,* **41**, 1903-1910,
637 https://doi.org/10.1016/j.atmosenv.2006.10.065, 2007.
638 Lin, Y.-C., Cheng, M.-T., Ting, W.-Y., and Yeh, C.-R.: Characteristics of gaseous
639 HNO_2, HNO_3, NH_3 and particulate ammonium nitrate in an urban city of central
640 Taiwan. *Atmos. Environ.,* **40**(25), 4725-4733,
641 https://doi.org/10.1016/j.atmosenv.2006.04.037, 2006.
642 Liu, M., Song, Y., Zhou, T., Xu, Z., Yan, C., Zheng, M., Wu, Z., Hu, M., Wu, Y., and
643 Zhu, T.: Fine particle pH during severe haze episodes in northern China.
644 *Geophys. Res. Lett.,* **44**, 5213-5222, https://doi.org/10.1002/2017GL073210,
645 2017.
646 Mental, T. F., Sohn, M., and Wahner, A.: Nitrate effect in the heterogeneous
647 hydrolysis of dinitrogen pentoxide on aqueous aerosols. *Phys. Chem. Chem.*
648 *Phys.*, **1**, 5451-5457, https://doi.org/10.1039/a905338g, 1999.

649 Nel, A.: Air pollution-related illness: effects of particles. *Science*, **308**, 804-806,
650 https://doi.org/10.1126/science.1108752, 2005.
651 Pan, Y., Tian, S., Zhao, Y., Zhang, L., Zhu, X., Gao, J., Huang, W., Zhou, Y., Song, Y.,
652 Zhang, Q., and Wang, Y.: Identifying ammonia hotspots in China using a national
653 observation work. *Environ. Sci. and Technol.*, **52**, 3926-3934.
654 https://doi.org/10.1021.acs/est.7b05235, 2018.
655 Pathak, R. K., Wu, W. S., and Wang, T.: Summertime $PM_{2.5}$ ionic species in four
656 major cities of China: nitrate formation in an ammonia-deficient atmosphere.
657 *Atmos. Chem. and Phys.*, **9**, 1711-1722, https://doi.org/10.5194/acp-9-1711-2009,
658 2009.
659 Pathak, R. K., Wang, T., and Wu, W. H.: Nighttime enhancement of $PM_{2.5}$ in
660 ammonia-poor atmospheric conditions in Beijing and Shanghai: Plausible
661 contributions of heterogeneous hydrolysis of N_2O_5 and HNO_3 partitioning.
662 *Atmos. Environ.,* **45**, 1183-1191, https://doi.org/10.1016/j.atmosenv.2010.09.003,
663 2011.
664 Polissar, A. V., Hopke, P. K., Paatero, P., Kaufmann, Y. J., Hall, D. K., Bodhaine, B.
665 A., Dutton, E. G., and Harris, J. M.: The aerosol at Barrow, Alaska: long-term
666 trends and source locations. Atmos. Environ., **33**, 2441-2458,
667 https://doi.org/10.1016/j.atmosenv.2018.08.0642, 2018.
668 Prabhakar, G., Parworth, C. L., Zhang, X., Kim, H., Young, D. E., Beyersdorf, A. J.,
669 Ziemba, L. D., Nowak, J. B., Bertram, T. H., Faloona, I. C., Zhang, Q., and
670 Cappa, C. D.: Observational assessment of the role of nocturnal residual-layer
671 chemistry in determining daytime surface particulate nitrate concentrations.
672 *Atmos. Chem. Phys.*, **17**, 14747-14770, https://doi.org/10.5194/acp-17-14747-
673 2017, 2017.
674 Squizzato, S., Masiol, M., Brunelli, A., Pistollato, S., Tarabotti, Z., Rampazzo, G., and

675 Pavoni, B.: Factors determining the formation of secondary inorganic aerosol: a
676 case study in the Po Valley (Italy). *Atmos. Chem. and Phys.,* **13**, 1927-1339,
677 https://doi.org/10.5194/acp-13-1927-2013, 2013.
678 Tang, X., Zhang, X., Ci, Z., Guo, J., and Wang, J.: Speciation of the major inorganic
679 salts in atmospheric aerosols of Beijing: China: measurements and comparison
680 with model. *Atmos. Environ.,* **133**, 123-134, https://doi.org/10.1016/j.atmosenv.
681 2016.03.013.
682 Tao, Y., Ye, X., Ma, Z., Xie, Y., Wang, R., Chen, J., Yang, X., and Jiang, S.: Insights
683 into different nitrate formation mechanisms from seasonal variations of secondary
684 inorganic aerosols in Shanghai. *Atmos. Environ.,* **145**, 1-9,
685 https://doi.org/10.1016/j.atmosenv.2016.09.012, 2016.
686 ten Brink, H., Otjes, R., Jongejan, P., and Slanina, S.: An instrument for semi-
687 continuous monitoring of the size-distribution of nitrate, ammonium, sulfate and
688 chloride in aerosols. *Atmos. Environ.,* **41**, 2768-2779,
689 https://doi.org/10.1016/j.atmosenv.2006.11.041, 2007.
690 Wahner, A., Mental, T. F., Sohn, M., and Stier, J.: Heterogenous reaction of N_2O_5 on
691 sodium nitrate aerosol. *J. Geophys. Res. Atmos.*, **103**, 31103-31112,
692 https://doi.org/10.1029/1998JD100022, 1998.
693 Wang, G., Wang, H., Yu, Y., Gao, S., Feng, J., Gao, S., & Wang, L.: Chemical
694 characterization of water-soluble components of PM_{10} and $PM_{2.5}$ atmospheric
695 aerosols in five locations of Nanjing, China. *Atmos. Environ.*, **37**., 2893-2902.
696 https://doi.org/10.1016/j.atmosenv.S1352-2310(03)00271-1, 2003.
697 Wang, G., Zhang, R., Geomez, M. E., Yang, L., Zamora, M. L., Hu, M., Lin, Y., Peng,
698 J., Guo, S., Meng, J., Li, J., Cheng, C., Hu, T., Ren, Y., Wang, Y., Gao, J., An, Z.,
699 Zhou, W., Li, G., Wang, J., Tian, P., Marrero-Ortiz, W., Secrest, J., Du, Z., Zheng,
700 J., Shang, D., Zheng, L., Shao, M., Wang, W., Huang, Y., Wang, Y., Zhu, Y., Li,

Y., Hu, J., Pan, B., Cai, L., Cheng, Y., Ji, Y., Zhang, F., Rosenfeld, D., Liss, P. S., Duce, R. A., Kolb, C. E., and Molina, M. J.: Persistent sulfate formation from London fog to Chinese haze. *Proc. Natl. Acad. Sci.*, **113**, 13630-13635, https://doi.org/ 10.1073/pnas.1616540113, 2016.

Wang, H., Lu, K., Chen, X., Zhu, Q., Chen, Q., Guo, S., Jiang, M., Li, X., Shang, D., Tang, Z., Wu, Y., Wu, Z., Zou, Q., Zheng, Y., Zheng, L., Zhu, T., Hu, M., and Zhang, Y.: High N_2O_5 concentrations observed in urban Beijing: implications of a large nitrate formation. *Environ. Sci. Technol. Lett.*, **4**, 416-420, https://doi.org/10.1021/acsestlett.7b00341, 2017.

Wang, H., Zhu, B., Shen, L., Xu, H., An, J., Xue, G., and Cao, J.: Water soluble ions in atmospheric aerosols measured in five sites in the Yantze River Delta, China: size-fractionated seasonal variation and sources. *Atmos. Environ.*, **123**(B), 370-379, https://doi.org/10.1016/j.atmosenv.2015.05.070, 2015.

Wang, W., Yu, J., Cui. Y., He, J., Xue, P., Cao, W., Ying, H., Gao, W., YIng, Y., Gao, W., Yan, Y., Hu, B., Xin, J., Wang, L., Liu, Z., Sun, Y., Ji, D., and Wang, Y.: Characteristics of fine particulate matter and its sources in an industrialized coastal city, Ningbo, Yantze River Delta, China. *Atmos. Res.*, **203**, 105-117, https://doi.org/10.1016/j.atmosres.2017.11.033, 2018.

Wang, Y., Zhuang, G., Zhang, X., Xu, C., Tang, A., Chen, J., and An, Z.: The ion chemistry, seasonal cycle, and sources of $PM_{2.5}$ and TSP aerosol in Shanghai. *Atmos. Environ.,* **40**(16), 2935-2952, https://doi.org/10.1016/j.atmosenv.2005.12.051, 2006.

Wei, L., Yue, S., Zhao, W., Yang, W., Zhang, Y., Ren, L., Han, X., Guo, Q., Sun, Y., Wang, Z., and Fu, P.: Stable sulfur isotope ratios and chemical compositions of fine aerosols ($PM_{2.5}$) in Beijing, China. *Sci. Total Environ.*, **633**, 1156-1164, https://doi.org/10.1016/j.scitotenv.2018.03.153, 2018.

727 Wen, L., Chen, J., Yang, L., Wang, X., Xu, C., Sui, X., Yao, L., Zhu, Y., Zhang, J.,
728 Zhu, T., and Wang, W.: Enhanced formation of particulate nitrate at a rural site on
729 the North China Plain in summer: the importance roles of ammonia and ozone.
730 *Atmos. Environ.,* **101**, 294-302, https://doi.org/10.1016/j.atmosenv.2014.11.037,
731 2015.
732 Yang, H., Yu, J. Z., Ho, S. S. H., Xu, J., Wu, W.-S., Wan, C. H., Wang, X., Wang, X.,
733 and Wang, L.: The chemical composition of inorganic and carbonaceous
734 materials in $PM_{2.5}$ in Nanjing, China. *Atmos. Environ. ,* **39**, 3735-3749,
735 https://doi.org/10.1016/j.atmosenv.2005.03.010, 2005.
736 Yao, X., Chan, C. K., Fang, M., Cadle, S., Chan, T., Mulawa, P., He, K., and Ye, B.:
737 The water-soluble ionic composition $PM_{2.5}$ in Shanghai and Beijing, China.
738 *Atmos. Environ.,* **36**, 4223-4234, https://doi.org/10.1016/j.atmosenv.2005.12.051,
739 2002.
740 Ye, X. N., Ma, Z., Zhang, J. C., Du, H. H., Chen, J. M., Chen, H., Yang, X., Gao, W.,
741 and Geng, F. H.: Important role of ammonia on haze formation in Shanghai.
742 *Environ. Res. Lett.*, **6**, 024019, https://doi.org/10.1088/1748-9326/6/2024019,
743 2011.
744 Ye, Z., Liu, J., Gu, A., Feng, F., Liu, Y., Bi, C., Xu, J., Li, L., Chen, H., Chen, Y., Dai,
745 L., Zhou, Q., and Ge, X.: Chemical characterization of fine particulate matter in
746 Changzhou, China and source apportionment with offline aerosol mass
747 spectrometry. *Atmos. Chem. .Phys.,* **17**, 2573-2592, https://doi.org/10.5194/acp-
748 17-2573-2017, 2017.
749 Zhang, R., Jing, J., Tao, J., Hsu, S.-C., Wang, G., Cao, J., Lee, C.S.L., Zhu, L., Chen,
750 Z., Zhao, Y., and Shen, Z., Chemical characterization and source apportionment
751 of $PM_{2.5}$ in Beijing: seasonal perspective. *Atmos. Chem. .Phys.,* **13**, 7053-7074,
752 https://doi.org/10.5194/acp-13-7053-20173, 2013.

753 Zhang, Y.-L., and Cao, F.: Fine particulate matters ($PM_{2.5}$) in China at a city level. *Sci.*
754 *Rep.,* **5**, 14884, https://doi.org/10.1038/srep14884, 2015.
755 Zhao, P. S., Dong, F., He, D., Zhao, X. J., Zhang, X. L., Zhang, W. Z., Yao, Q., and
756 Liu, H. Y.: Characteristics of concentrations and chemical compositions for
757 PM2.5 in the region of Beijing, Tianjin, and Hebei, China. *Atmos. Chem. Phys.,*
758 **13**, 4631-4644, https://doi.org/10.5194/acp-13-4631-2013, 2013.
759 Zheng, B., Tong, D., Li, M., Liu, F., Hong, C., Geng, G., Li, H., Li, X., Peng, L., Qi,
760 J., Yan, L., Zhang, Y., Zhao, H., Zheng, Y., He, K., and Zhang, Q.: Trends in
761 China's anthropogenic emissions since 2010 as the consequence of clean air
762 actions. *Atmos. Chem. .Phys.,* **18**(19), 14095-14111, https://doi.org/10.5194/acp-
763 18-14095-2018, 2018.
764 Zou, J., Liu, Z., Hu, B., Huang, X., Wen, T., Ji, D., Liu, J., Yang, Y., Yao, and Wang,
765 Y.: Aerosol chemical compositions in the Northern China Plain and the impact on
766 visibility in Beijing and Tianjin., *Atmos. Res.*, **201**, 235-246,
767 https://doi.org/10.1016/j.atmosres.2017.09.014, 2018.
768

Table Captions

Table 1 The regression models between NO_3^-/SO_4^{2-} (Y) and NH_4^+/SO_4^{2-} (X) along with the criterion values of NH_4^+/SO_4^{2-} in ammonium-rich regime during the sampling periods.

Figure Captions

Figure 1 Time series of concentrations in (a) $PM_{2.5}$ mass, (b) SIA species, (c) ALWC and (d) Ox along with (e) Fn observed in Nanjing during the sampling periods. The grey shadows represent the high $PM_{2.5}$ periods discussed in the section 3.6.

Figure 2 Abundance of each species in TWSIIs during the (a) entire, (b) haze ($PM_{2.5} \geq 150$ μg m^{-3}) and (c) clear ($PM_{2.5} < 35$ μg m^{-3}) events. The numbers in the parentheses are standard deviations.

Figure 3 Abundance of each species in TWSIIs during the (a) entire, (b) haze ($PM_{2.5} \geq 150$ μg m^{-3}) and (c) clear ($PM_{2.5} < 35$ μg m^{-3}) events. The numbers in the parentheses are standard deviations.

Figure 4 The PSCF maps of high nitrate pollution.

Figure 5 Scatter plots of molar ratios of NO_3^-/SO_4^{2-} against NH_4^+/SO_4^{2-} in Nanjing during the different seasons.

Figure 6 Scatter plot of NO_3^- vs. excess-NH_4^+ molar concentrations in Nanjing during the different seasons. The results in Beijing, Shanghai, Guangzhou, Lanzhou and Hong Kong are also shown in this figure.

Figure 7 Scatter plots of (a) Fn against Ox and (b) Fn against ALWC in daytime and nighttime aerosol samples during the high hourly $PM_{2.5}$ concentration conditions (hourly $PM_{2.5} \geqq 150$ μg m^{-3}).

Figure 8 Time series of concentrations in (a) $PM_{2.5}$ mass and CO, (b) SIA species

795 (NO_3^-, SO_4^{2-} and NH_4^+), (c) ALWC, Ox and NO_2 and (d) RH and T in
796 Nanjing City from March 3 to 6, 2016. The grey shadows denote $PM_{2.5}$
797 episodes. The red numbers represent NO_3^- production rate during the $PM_{2.5}$
798 episodes.
799 Figure 9 Nitrate concentrations simulated by ISORROPIA II model dependening on
800 TN and TA concentrations under (a) SO_4^{2-} = 10 μg m^{-3} and (b) SO_4^{2-} = 60
801 μg m^{-3}. The purple dots denote the observed TN and TA concentrations at
802 the receptor site during the sampling periods.
803

Table 1 The regression models between NO_3^-/SO_4^{2-} (Y) and NH_4^+/SO_4^{2-} (X) along with the criterion values of NH_4^+/SO_4^{2-} in ammonium-rich regime during the sampling periods.

Sampling periods	Regression models	Criterion values of NH_4^+/SO_4^{2-}
2016 spring	$Y = 0.71\ X - 1.27;\ R^2 = 0.87$	1.8
2016 summer	$Y = 0.67\ X - 1.22;\ R^2 = 0.86$	1.8
2017 winter	$Y = 0.81\ X - 1.50;\ R^2 = 0.91$	1.9
2017 spring	$Y = 0.95\ X - 1.91;\ R^2 = 0.94$	2.0
2017 summer	$Y = 0.79\ X - 1.32;\ R^2 = 0.84$	1.7

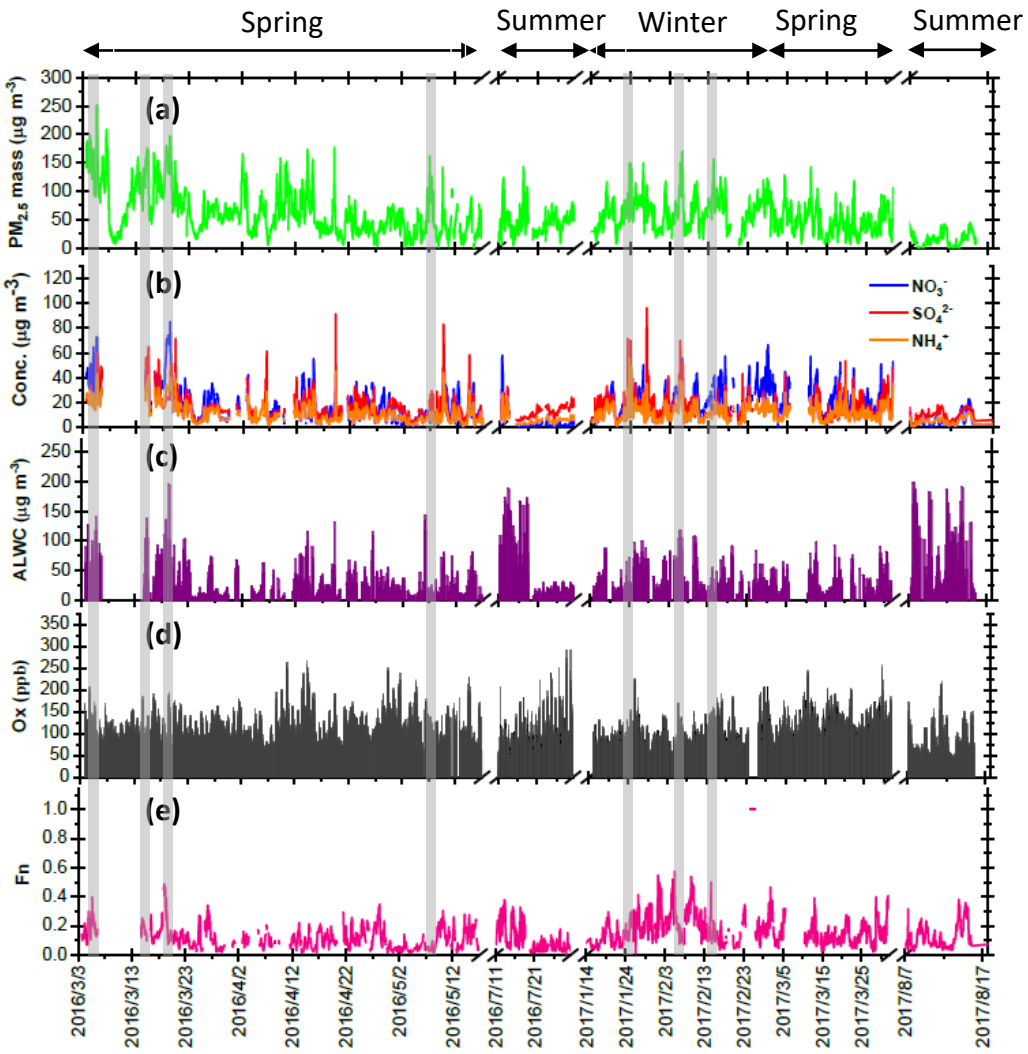

Figure 1 Time series of concentrations in (a) $PM_{2.5}$ mass, (b) SIA species, (c) ALWC and (d) Ox along with (e) Fn observed in Nanjing during the sampling periods. The grey shadows represent the high $PM_{2.5}$ periods discussed in the section 3.6.

(a) Entire days: $PM_{2.5}$ = 58 ± 35 μg m^{-3}

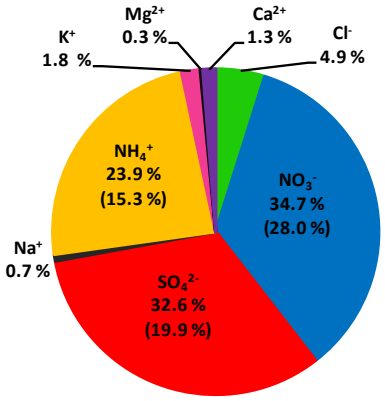

(b) Haze events: $PM_{2.5}$ = 171 ± 18 μg m^{-3}

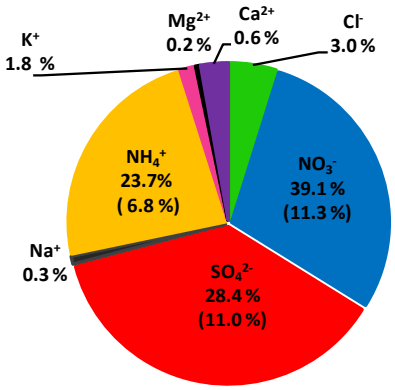

(c) Clear events: $PM_{2.5}$ = 22 ± 9 μg m^{-3}

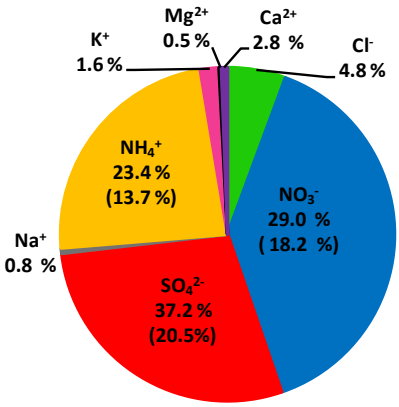

Figurer 2 Abundance of each species in TWSIIs during the (a) entire, (b) haze ($PM_{2.5}$ ≥ 150 μg m^{-3}) and (c) clear ($PM_{2.5}$ < 35 μg m^{-3}) events. The numbers in the parentheses are standard deviations.

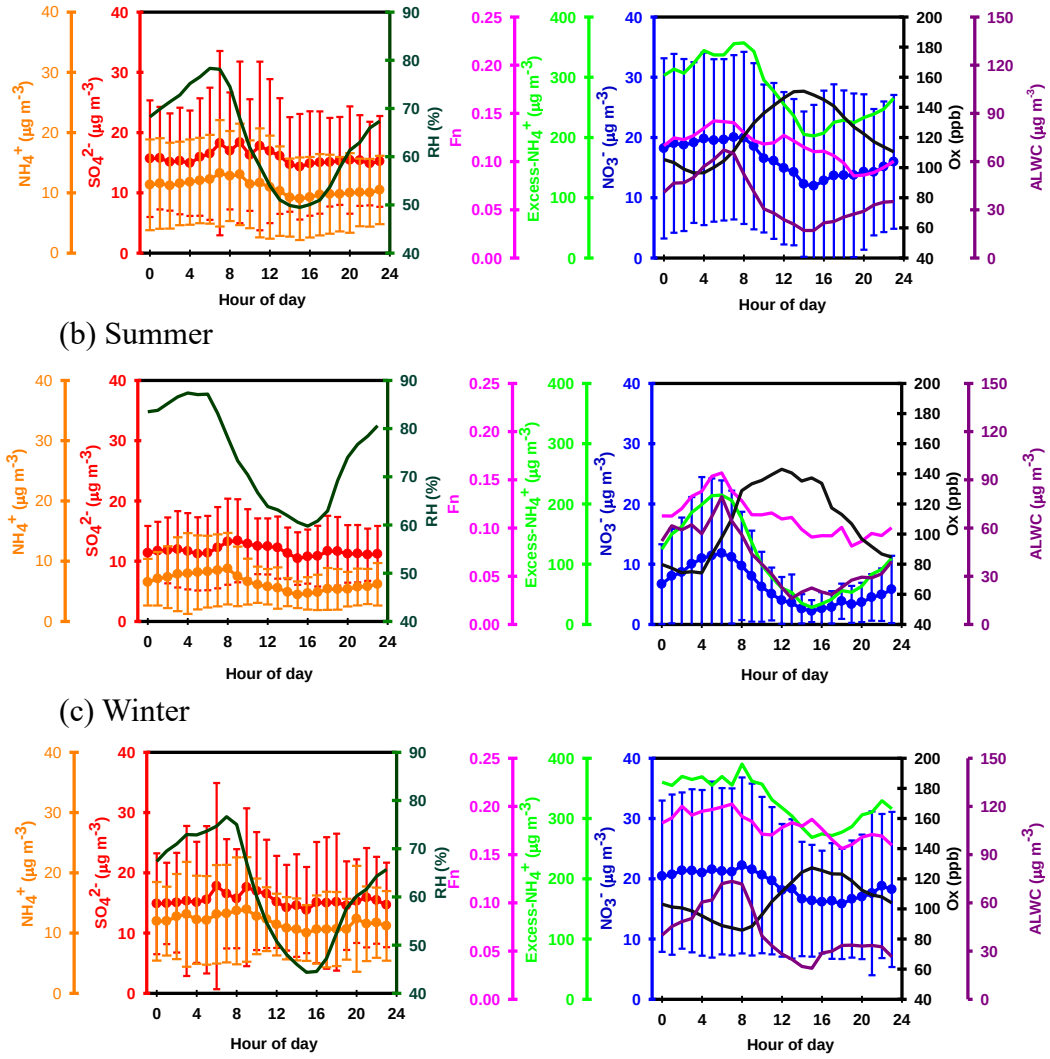

Figure 3 Diurnal variations of the concentrations of NO_3^-, SO_4^{2-} and NH_4^+, excess-NH_4^+, Ox and ALWC, and nitrogen conversion ratio (Fn) as well as ambient relative humidity in Nanjing during the sampling periods. For SO_4^{2-}, NO_3^- and NH_4^+, the mean values (dots) and standard deviations (solid lines) are plotted.

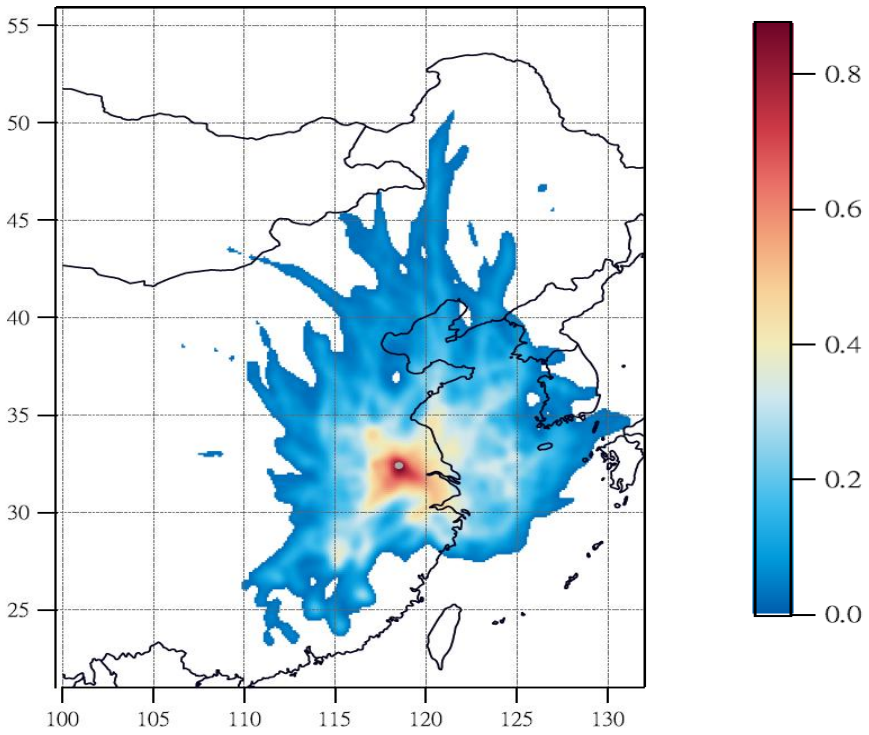

Figure 4 The PSCF maps of high nitrate pollution.

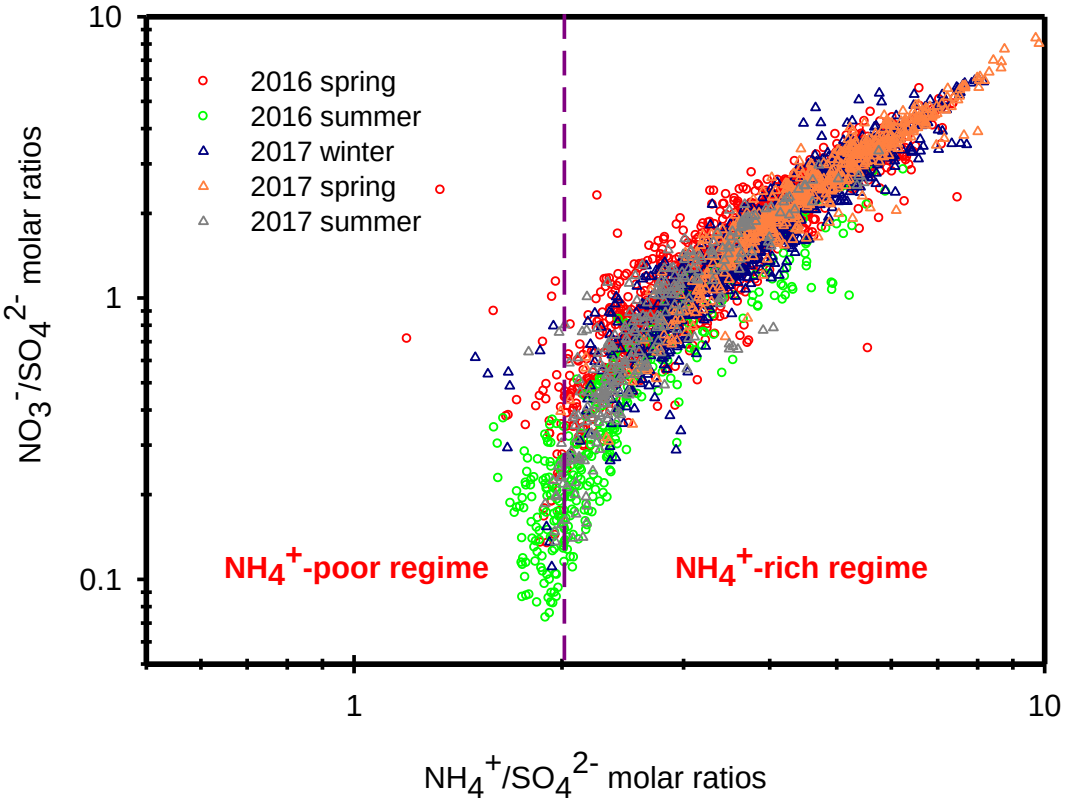

Figure 5 Scatter plots of molar ratios of NO_3^-/SO_4^{2-} against NH_4^+/SO_4^{2-} in Nanjing during the different seasons.

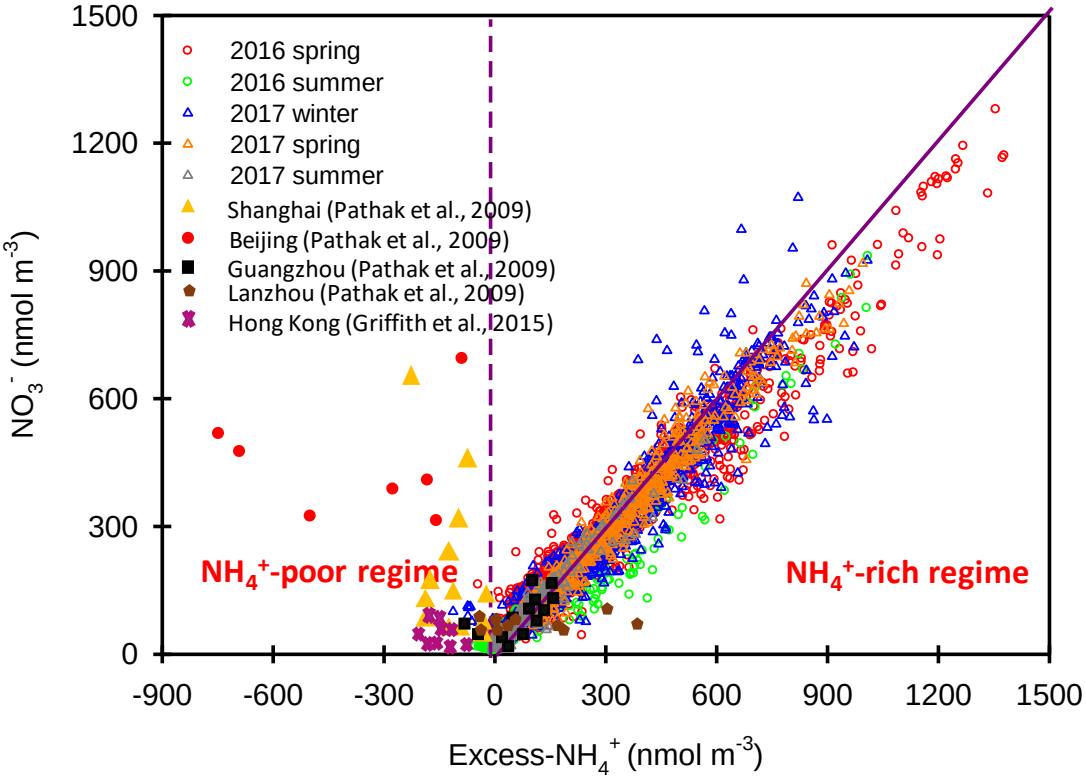

Figure 6 Scatter plot of NO_3^- vs. excess-NH_4^+ molar concentrations in Nanjing during the different seasons. The results in Beijing, Shanghai, Guangzhou, Lanzhou and Hong Kong are also shown in this figure.

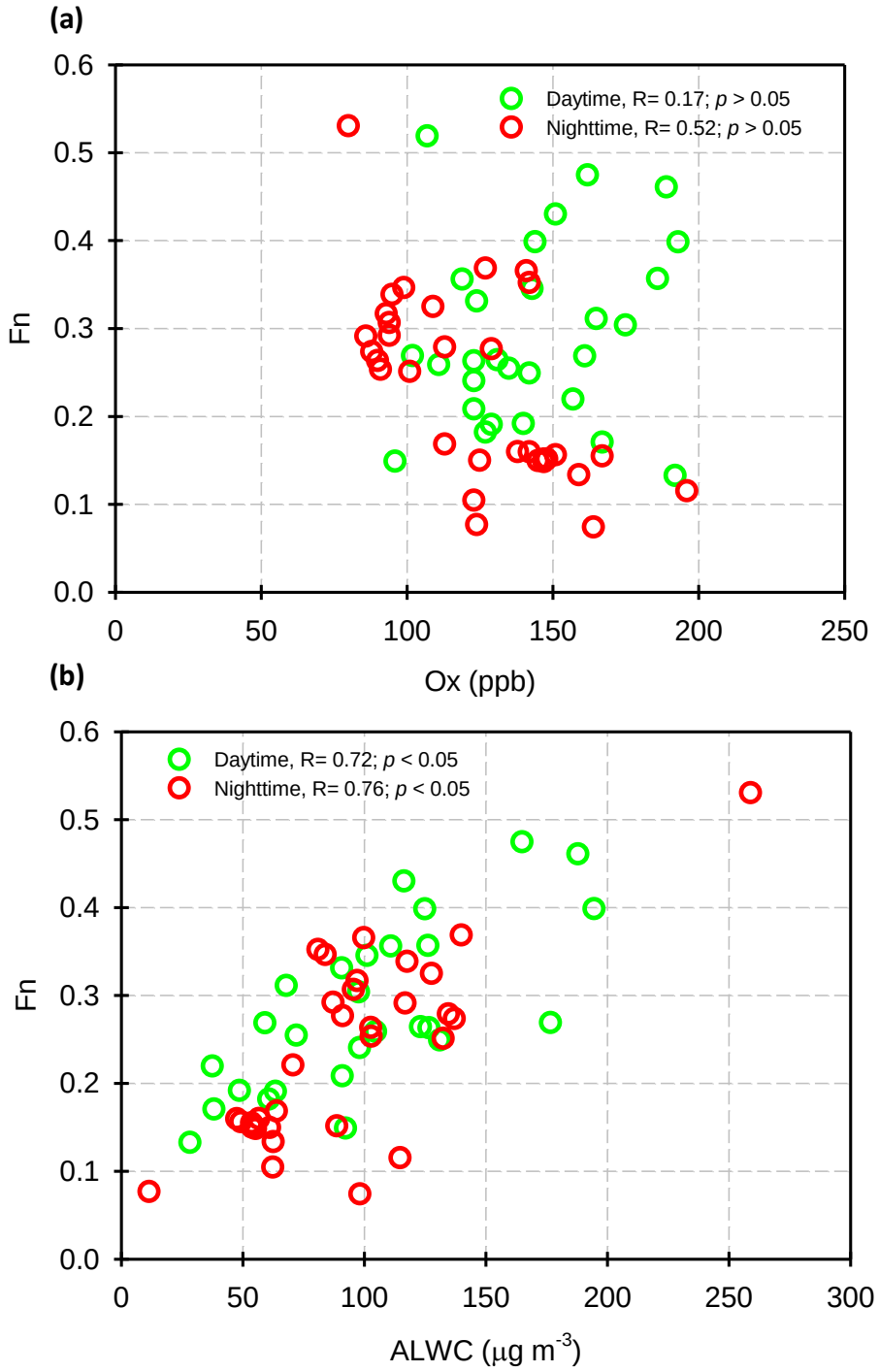

Figure 7 Scatter plots of (a) Fn against Ox and (b) Fn against ALWC in daytime and nighttime aerosol samples during the high hourly $PM_{2.5}$ concentration conditions (hourly $PM_{2.5}$ $\geqq$ 150 μg m^{-3}).

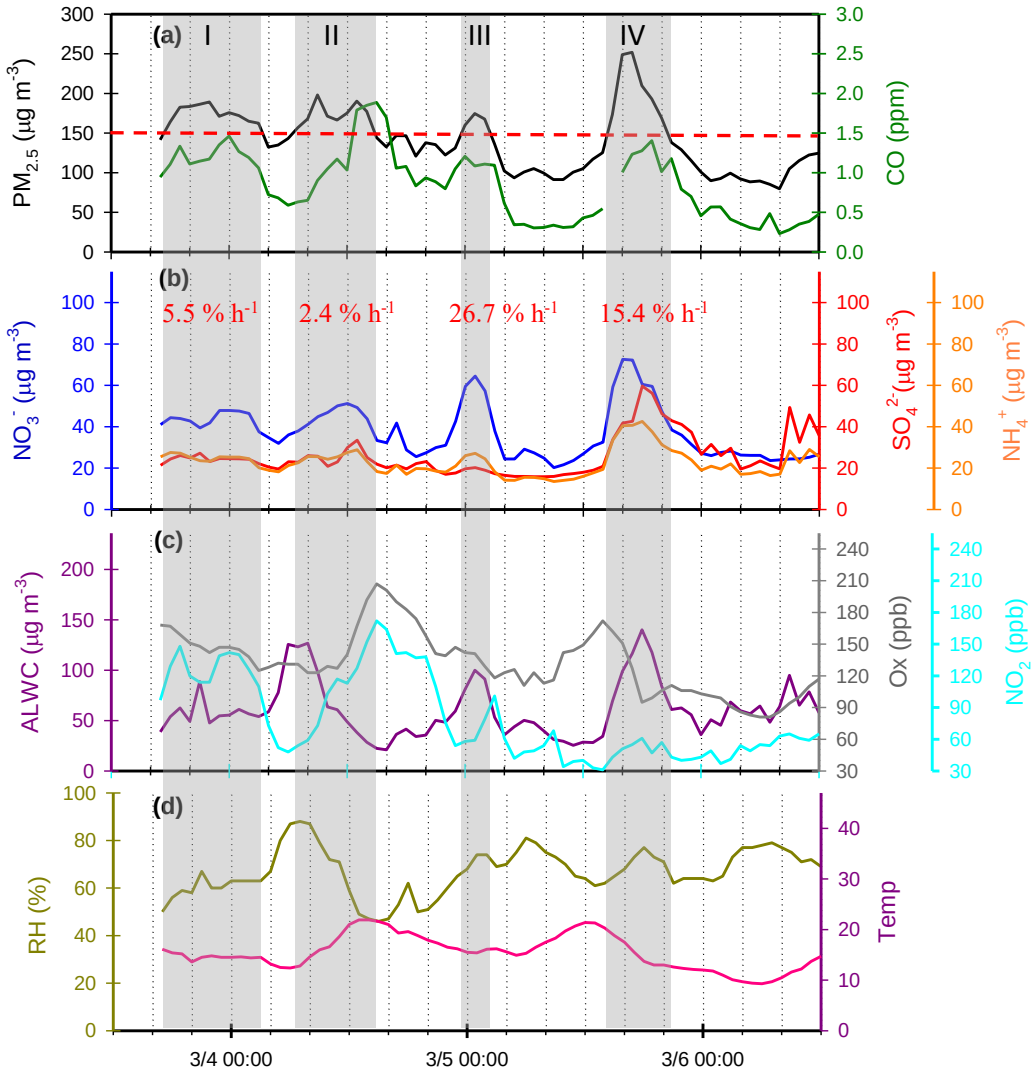

Figure 8 Time series of concentrations in (a) $PM_{2.5}$ mass and CO, (b) SIA species (NO_3^-, SO_4^{2-} and NH_4^+), (c) ALWC, Ox and NO_2 and (d) RH and T in Nanjing City from March 3 to 6, 2016. The grey shadows denote $PM_{2.5}$ episodes. The red numbers represent NO_3^- production rate during the $PM_{2.5}$ episodes.

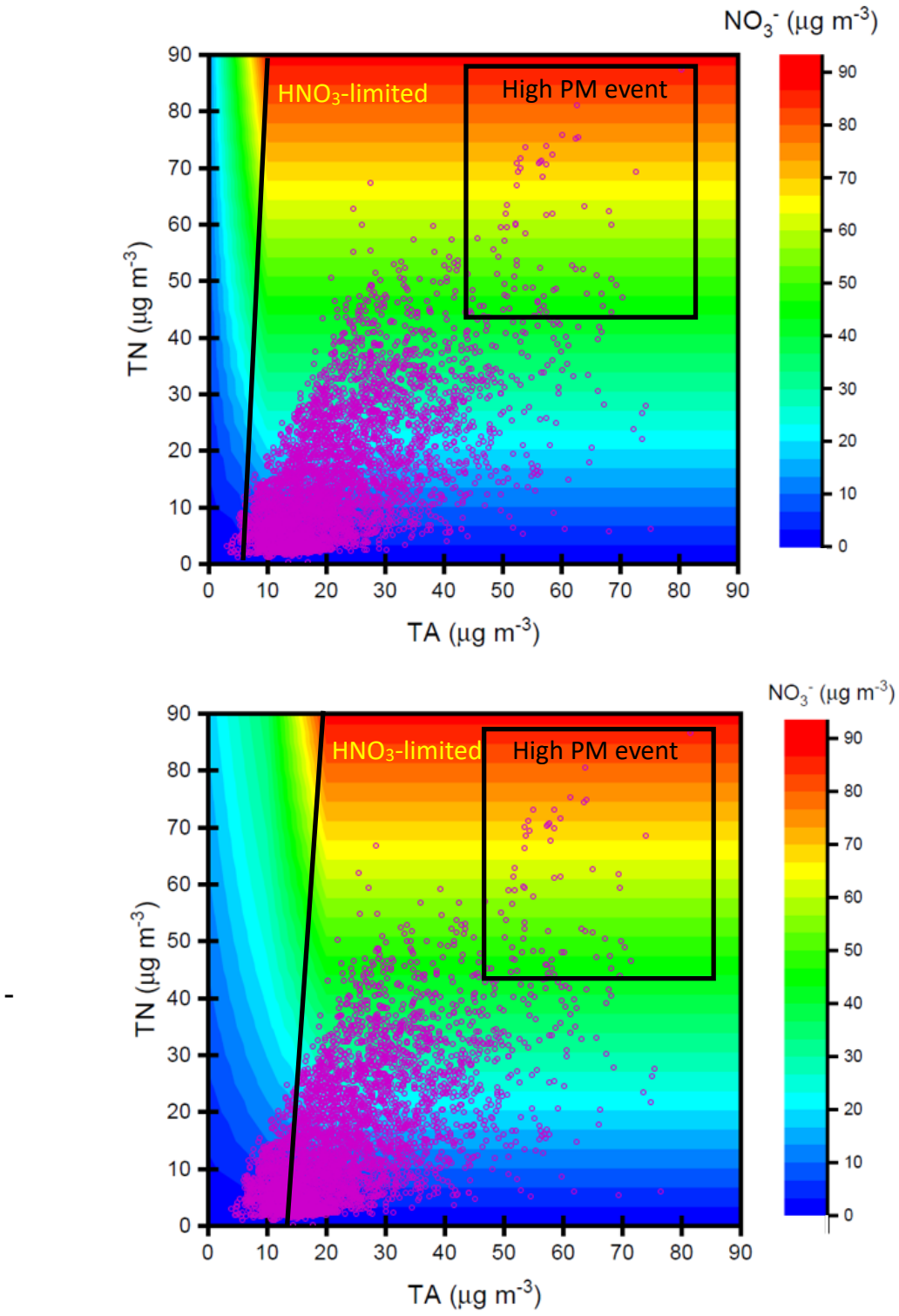

Figure 9 Nitrate concentrations simulated by ISORROPIA II model depending on TN and TA concentrations under (a) SO_4^{2-} = 10 μg m^{-3} and (b) SO_4^{2-} = 60 μg m^{-3}. The purple dots denote the observed TN and TA concentrations at the receptor site during the sampling periods.